A SIMPLE PROGNOSTIC CLOSURE ASSUMPTION TO DEEP CONVECTIVE PARAMETERIZATION: II

Chen Dehui (陈德辉) and *Philippe Bougeault*

Centre National de Recherche Météorologique, 31057 Toulouse Cédex, France

Received August 29, 1992; revised October 12, 1992

ABSTRACT

A series of 3D predictions, dealing with the development of a heavy storm observed during the OSCAR experiment, were carried out by utilizing the PERIDOT model, and introducing alternatively the cumulus parameterization scheme of Bougeault (1985) and the prognostic one (Chen, 1989; Chen and Bougeault, 1993), with three different grid sizes: 160 km, 80 km, 40 km. The feasibility of the new prognostic scheme and its improvement on the problem of dependency of the predicted rainfall upon the grid size of the numerical model were verified by comparison of the rainfall observed and those predicted.

The results demonstrate that, in general, the predicted rainfall increases when the grid size decreases for both diagnostic and prognostic schemes. However, with the new prognostic scheme, the numerical model is capable, on the one hand, for the larger grid sizes, to increase the rainfall, which is under–estimated with the scheme of Bougeault (1985); on the another hand, for the smaller grid sizes, to reduce the rainfall, which is usually over–estimated. In other word, there is an obvious improvement on the problem under study.

Key words: prognostic closure assumption, convection parameterization, 1D experiment, sensitivity experiment

I. INTRODUCTION

In the companion paper (Chen and Bougeault, 1993), we have developed a new prognostic cumulus parameterization scheme, which is theoretically based on an idea that a cumulus parameterization scheme adaptable to some numerical weather prediction (NWP) models with very small mesh must rely upon prognostic convective quantities representing the cumulus activity, and a suitable closure assumption. We have presented the semi–prognostic tests with a one–dimensional experiment in comparison with the observational dataset of Phase III of GATE. The new scheme stability and consistency with the dynamic model, and its good agreement with the observational dataset have been established.

However, the assessment of the scheme in three–dimensional experiments is much more interesting for the feasibility in prediction, because it is an important problem whether the cumulus parameterization scheme is coherent or not with the whole NWP model, including all other physical parameterization schemes. In addition, since the ultimate purpose of our work is to study and to attempt to resolve the problem of the predicted rainfall sensibility to the grid size of the numerical model, and since the forcing environment and the grid size are assumed to be " stationary" in one–dimensional experiments as usually done, a complete investigation in three–dimensional experiments is indeed necessary.

Some investigations of the prognostic scheme with a new closure assumption (Eq. (19), Chen and Bougeault, 1993, CB2 for short hereinafter) are presented in Section III after a brief description of the NWP model and the dataset used in Section II. A conclusion of the three–dimensional experiment results is given in Section IV.

II. 3D EXPERIMENTS

In order to establish the feasibility of the new prognostic scheme, and to evaluate its efficiency in a real case for resolving the problem of dependence of the predicted rainfall upon the grid size, we have run the PERIDOT model (PERIDOT is the name for the French fine mesh limited area operational model). Including alternatively the prognostic scheme and the B85 (Bougeault, 1985) scheme, the forecasts were produced for a case of heavy storm development and with different grid sizes: 160 km, 80 km, 40 km.

The results of our two–dimensional experiments (Chen, 1989) showed that, although the prognostic approach did reduce the sensitivity of the rainfall to the grid size, but is not sufficient to cancel it, because the model, with the hydrostatic approximation, could induce still too large scale circulation which may generate more precipitations for the smaller grid size ($\triangle x < 100$ km). Finally, we did find that the prognostic scheme, with the new closure assumption for the Rate of Moisture Convergence (RMC, Eq. (19), CB2), gave better results. So, we have introduced the CB2 scheme for the three–dimensional experiments. The essential results will be reported in next section.

1. *PERIDOT Model and OSCAR Dataset*

The PERIDOT model is both in operational use (since the beginning of 1985) for producing every day forecasts over France and its immediate surroundings, and in research use for the mesoscale numerical experiments. A detailed description of the model is given in Imbard et al. (1987), and Geleyn et al. (1988). Here are some main features: Nonlinear normal mode initialization (Brière, 1982); Dynamic: 15 σ–levels with the usual vertical staggering among the dynamic and thermodynamic variables, and an Arakawa C–grid for horizontal fields; Davies technique for lateral boundary conditions (Davies, 1976); semi–implicit leap–frog scheme; ^{2} horizontal diffusion; Envelope orography: $m+\sqrt{2}\cdot\sigma'$ (with m mean value and σ' standard deviation as deduced from the $16'\times 16'$ US Navy data); Physics: Kessler type evaporation of rainfall for large–scale condensation (the excess water vapour beyond limit saturation condenses and falls out as large–scale condensation); Kuo–type scheme for deep convection (Geleyn, 1985); ECMWF–type scheme for PBL parameterization (Louis, 1979); Modified Richardson Number's approach for parameterizing the effects of shallow convection (Geleyn, 1986).

The OSCAR (Oxidation and Scavenging Characteristics of April Rain) dataset was provided by NCAR for the period from 00 GMT 22 April to 00 GMT 25 April 1981, every 12 hours. It covers a domain 46×61 points with $\triangle x = 160$ km over the Southeast of United States (Fig. 1), and contains 14 standard pressure levels for temperature, relative humidity and winds. The domain was projected by a conform Lambert method and centered at 90°W, 40°N. This dataset was interpolated into grid points of PERIDOT model by Degardin and Imbard (1987). They have used these analysed data to produce forecasts with PERIDOT model for taking part in an intercomparison project between different mesoscale models proposed by NCAR.

2. *Description of Experiments*

(1) *Some modifications*

The PERIDOT model was run in our experiments with some modifications: The horizontal diffusion was estimated in ^{4}(instead of ^{2}); the scheme of shallow convection was taken off for avoiding unusable complication of the problem; the scheme of deep convection was replaced alternatively by the B85 scheme and the CB2 scheme; the 15 σ–levels of the EMERAUDE model was introduced (EMERAUDE is the name for another French spectrum large–scale operational model).

(2) *Nested domains*

Three different grid sizes ($\triangle x$ = 160 km, 80 km, 40 km) were used for investigating the problem of dependence of the predicted rainfall upon the grid size. Their "nested" domains of experiments are shown in Fig. 1. The area average rainfall over the controlling domain $\overline{R}_p$ was

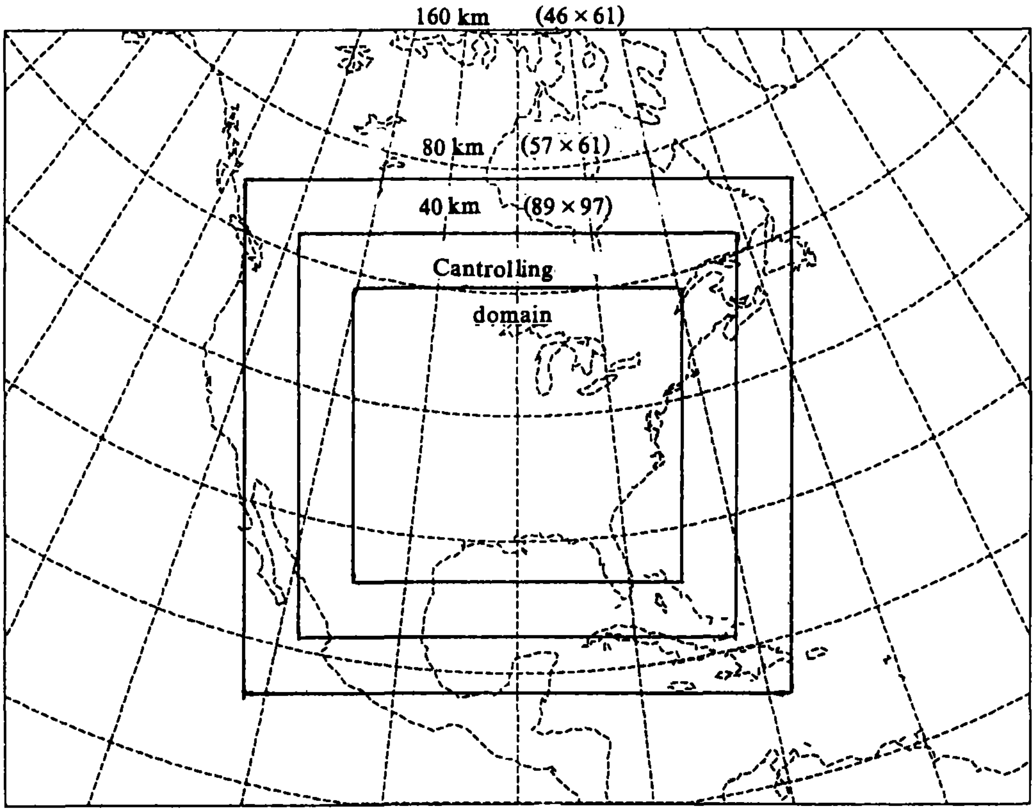

Fig. 1. Nested domains of the predictions with different grid scales, utilizing the experiment OSCAR data. The largest box is for the predictions with grid scale $\triangle x$ = 160 km (grid pionts: 46 × 61); the second box with $\triangle x$ = 80 km (grid pionts: 57 × 61); the third box with $\triangle x$ = 40 km (grid pionts: 89 × 97); the smallest box is a controlling domain for the area average rainfall.

estimated by

$$\overline{R}_p = \frac{1}{\triangle S} \cdot \sum_{i,j=1}^{n_i,n_j} R_p(i,j) \cdot \triangle x_{i,j}^2, \tag{1}$$

where $R_p(i, j)$ denotes the rainfall accumulated over 24 hours at a given grid point (i, j); n_i, n_j the grid point numbers in X, Y axes of the controlling domain; $\triangle S(=\sum_{i,j=1}^{n_i,n_j} \triangle x_{i,j}^2)$ the total area of controlling domain (i. e., for grid size $\triangle x = 160$ km, $n_i = 19$, $n_j = 17$, $\triangle S \approx 8\ 268\ 800$ km^2). The controlling domain is identical for all different grid sizes ($\triangle x = 160$ km, 80 km, 40 km) so that the area average rainfall $\overline{R}_p$ can be comparable.

(3) *Initial data*

All experiments for $\triangle x = 160$ km were initialized to produce a 48–h forecast from 00 GMT 22 April to 00 GMT 24 April 1981, with the same analysed data as those Degardin and Imbard (1987) have used. Each series of experiments ($\triangle x = 160$ km$\rightarrow\triangle x = 80$ km$\rightarrow\triangle x = 40$ km) was run in a so–called "nested" way (Figs. 1 and 2). The analysed data files were used as input–files only for the forecasts with $\triangle x = 160$ km. The predicted data files with $\triangle x = 160$ km were used as input–files for the forecasts with $\triangle x = 80$ km. The predicted data files with $\triangle x = 80$ km were used as input–files for the forecasts with $\triangle x = 40$ km. Forecasts with $\triangle x = 80$ km, 40 km started in 12 hours later (at 12 GMT 22 April) for avoiding the effects of spin up.

(4) *Coefficient C_β*

It is a difficult choice for the C_β coefficient. At the present time, it was determined in an empirical way subject to certain constraints requiring reasonable area average predicted rainfall. We supposed:

$$C_\beta = \left(\frac{\triangle x}{\triangle x_0}\right)^a, \tag{2}$$

where a is a non–dimensional parameter to be determined; $\triangle x$ the grid size of the host model (in km); $\triangle x_0$ the grid size of reference. Theoretically, when $\triangle x \rightarrow \triangle x_0$, $C_\beta \rightarrow 1$. In this case, the NWP model would give better forecast. In fact, Table 2 showed that $\overline{R}_p$ obtained with the prognostic scheme, where $C_\beta = 1$ (CB1, in the following), $\triangle x = 80$ km, is nearly equal to observation: 5.05 mm (prediction) against 5.02 mm (observation). Thus, we consider: $\triangle x_0 \approx 80$ km. For the parameter a, we optimized it by some test predictions. Our 2D experiments (Chen, 1989) and 3D experiments (Chen, 1991) demonstrated that its value could be between 1—2. Finally, we took $a = 2$, that is

$$C_\beta = \left(\frac{\triangle x}{80}\right)^2. \tag{3}$$

It is obvious here that when the grid size of the host model is different from 80 km, the C_β coefficient may be superior or inferior to 1. When $C_\beta > 1$, it is found for the same justification as Krishnamurti et al. (1983); when $C_\beta < 1$, it means to decrease the vertical moisture advection (so, RMC) generated by the grid–scale circulations $(\overline{\omega})$, which usually are also induced in a mesoscale hydrostatical approximation model. Finally, with this formulation Eq. (3), we obtained better forecasts.

Analysed data (160 km)

22 / 04 / 1982 at 00 GMT (00h)
22 / 04 / 1982 at 12 GMT (12h)
23 / 04 / 1982 at 00 GMT (24h)
23 / 04 / 1982 at 12 GMT (36h)
24 / 04 / 1982 at 00 GMT (48h)

↓

Forecasts (160 km)

Input (160 km) 00h–12h–24h–36h–48h
Output (160 km) 00h–12h–24h–36h–48h

↓

Interpolation

Input (160 km) 00h–12h–24h–36h–48h
Output (80 km) 00h–12h–24h–36h

↓

Forecasts (80 km)

Input (80 km) 00h—12h—24h—36h
Output (80 km) 00h–06h–12h–18h–24h–30h–36h

↓

Interpolation

Input (80 km) 00h–06h–12h–18h–24h–30h–36h
Output (40 km) 00h–06h–12h–18h–24h–30h–36h

↓

Forecasts (40 km)

Input (40 km) 00h—06h—12h—18h—24h—30h—36h
Output (40 km) 00h–03h–06h–09h–12h–15h–18h–21h–24h–27h–30h–33h–36h

Fig. 2. Flow diagram of the experiments with different grid scales.

Table 1. Brief Summary of the Experiments with Different Grid Scales and Different Convective Parameterization Schemes

Schemes	No. exp.	Grid–sizes (km)	Ranges (h)	C_f	C_β
B85	1101	160	48	—	—
B85	1102	80	36	—	—
B85	1103	40	36	—	—
CB1	3111	160	48	50	1
CB1	3112	80	36	50	1
CB1	3113	40	36	50	1
CB2	6301	160	48	50	$(\triangle x / 80)^2$
CB2	6302	80	36	50	$(\triangle x / 80)^2$
CB2	6303	40	36	50	$(\triangle x / 80)^2$

III. RESULTS

A brief summary of the experiments is given in Table 1. We note that the Kuo–type scheme, used every day for the operational PERIDOT, was not compared here with the new prognostic scheme, but the latter was done only with the B85 scheme, because the results for the same case obtained by Degardin and Imbard (1987) indicated that the B85 scheme was better adapted to the case chosen than the Kuo–type scheme.

1. *Analysed Meteorological Situation*

This case was chosen for several times: either by Kuo et al. (1985) for testing the accuracy of trajectory models, or by Degardin and Imbard (1987) for assessing the PERIDOT model of the French Weather Service. A brief summary of this case was given by Kuo et al. (1985). During the period of 22—25 April 1981, one could observe a passage of cyclone, named OSCAR storm (Kuo et al., 1985), associated with a cold front system over the southwestern to

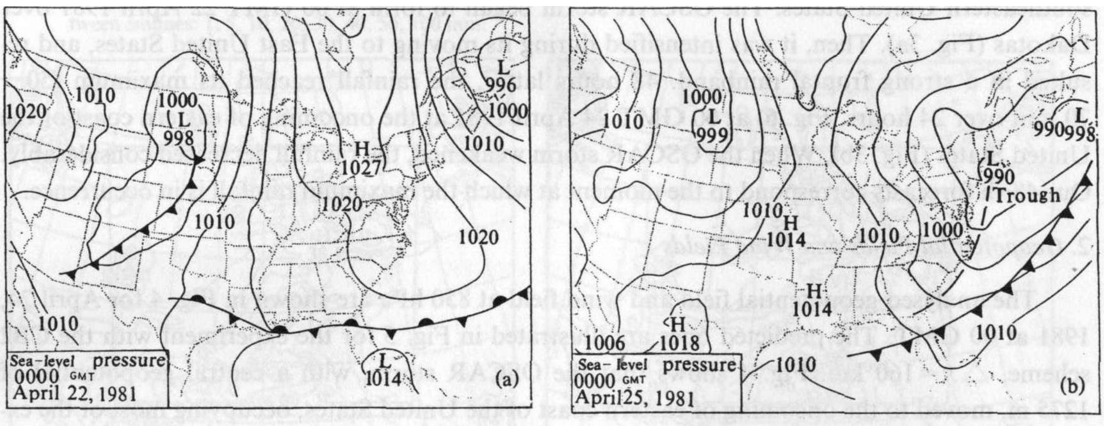

Fig. 3. Sea level pressure analysis field during the experiment OSCAR (from Kuo et al., 1985): (a) at 00 GMT 22 April 1981; (b) at 00 GMT 25 April 1981.

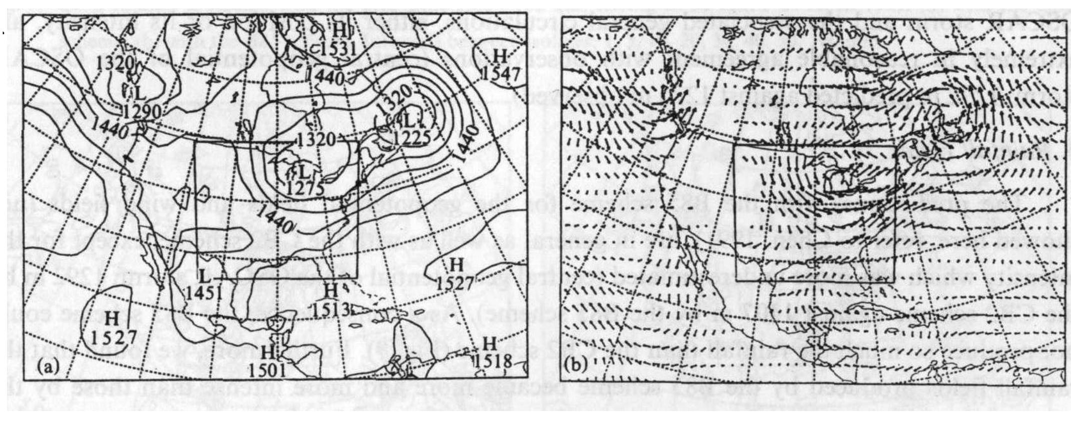

Fig. 4. 850 hPa analysis at 00 GMT 24 April 1981: (a) geopotential field; (b) wind field.

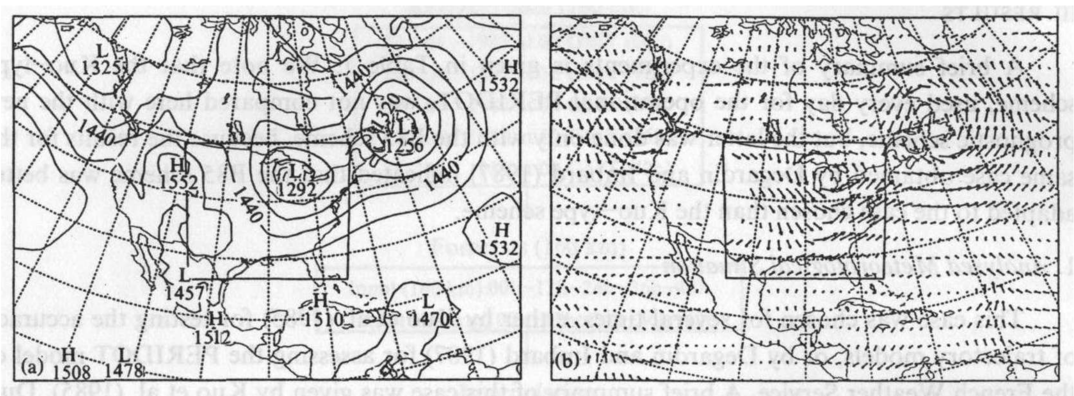

Fig. 5. As in Fig. 4, but for 48 h forecast, starting at 00 GMT 22 April 1981, with the grid scale $\triangle x = 160$ km and the CB2 scheme.

southeastern United States. The OSCAR storm began to form at 00 GMT 22 April 1981 over Dakotas (Fig. 3a). Then, it was intensified during its moving to the East United States, and resulted in a strong frontal rainband. 48 hours latter, the rainfall reached its maximum (50—70 mm over 24 hours, Fig. 6) at 00 GMT 24 April 1981 at the oncoming of eastern coast of the United States (Fig. 3b). When the OSCAR storm weakened, the rainfall decreased considerably. Our 48–h forecasts correspond to the moment at which the maximum rainfall is in occurrence.

2. *Geopotential Fields and Wind Fields*

The analysed geopotential field and wind field at 850 hPa are shown in Fig. 4 for April 24, 1981 at 00 GMT. The predicted ones are illustrated in Fig. 5 for the experiment with the CB2 scheme, $\triangle x = 160$ km. Fig. 4 shows that the OSCAR storm, with a central geopotential of 1275 m, moved to the oncoming of eastern coast of the United States, occupying most of the experiment's controlling domain. This synoptical situation in low altitude could be characterized by another strong marine cyclone (nearly unmovable) at the northeastern of the OSCAR storm. A comparison of Figs. 4 and 5 clearly shows that the predictions, with the CB2 scheme, of the OSCAR storm and the associated general circulations, either its position or its intensity, are extremely in reasonable agreement with observations (central geopotential of the OSCAR storm: 1292 m predicted against 1275 m observed).

3. *Rainfall Fields*

The predictions, with the B85 scheme for the geopotential fields and wind fields (not showed here, refer to Chen, 1991), are in general as well as with the CB2 scheme, except for the intensity which was more underestimated (central geopotential of the OSCAR storm: 1292 m by the CB2 scheme against 1307 m by the B85 scheme). As a consequence, the B85 scheme could not produce so much the rainfall than the CB2 scheme (Fig. 7). Furthermore, we found that the rainfall fields produced by the B85 scheme became more and more intense than those by the CB2 scheme when the grid sizes decrease (Figs. 7, 8 and 9), although the rainband inside the controlling domain was, as well as in both schemes, made close to the observed one

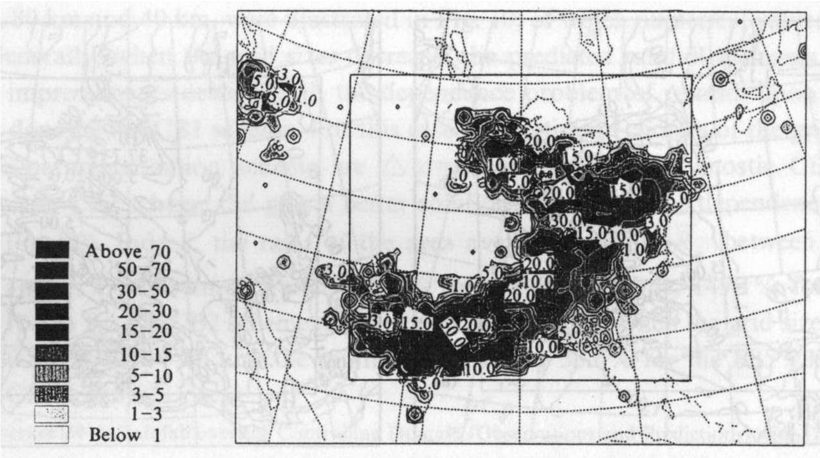

Fig. 6. 24–h rainfall observed during the experiment OSCAR, ending at 00 GMT 24 April 1981 (provided by Lawnam). The domain of observation corresponds to the prediction domain with $\triangle x = 80$ km (see Fig. 1). Intervals between isolines: 1, 5, 10, 20, 30, 40, 50, 100 mm.

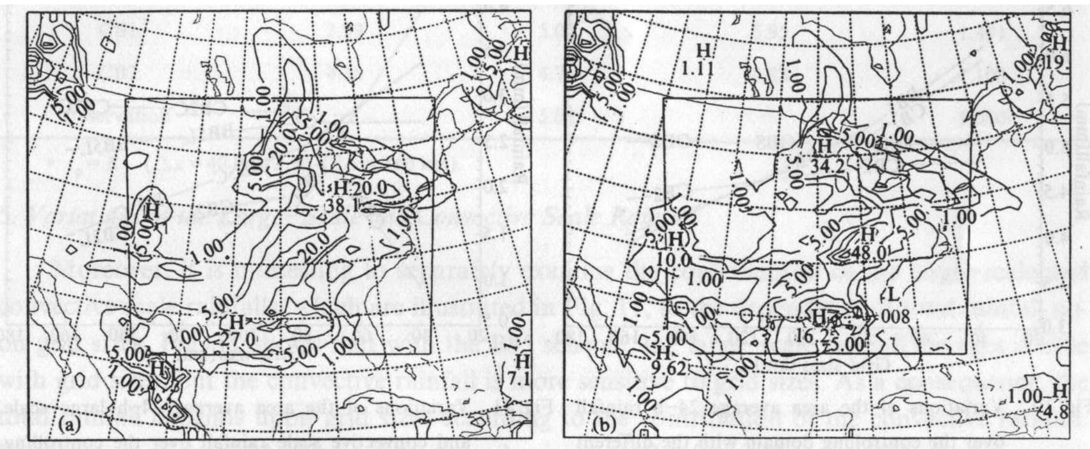

Fig. 7. 24–h rainfall predicted with the grid scale $\triangle x = 160$ km, ending at 00 GMT 24 April 1981: (a) with the CB2 scheme; (b) with the B85 scheme. Intervals between isolines: 1, 5, 10, 20, 30, 40, 50, 100 mm.

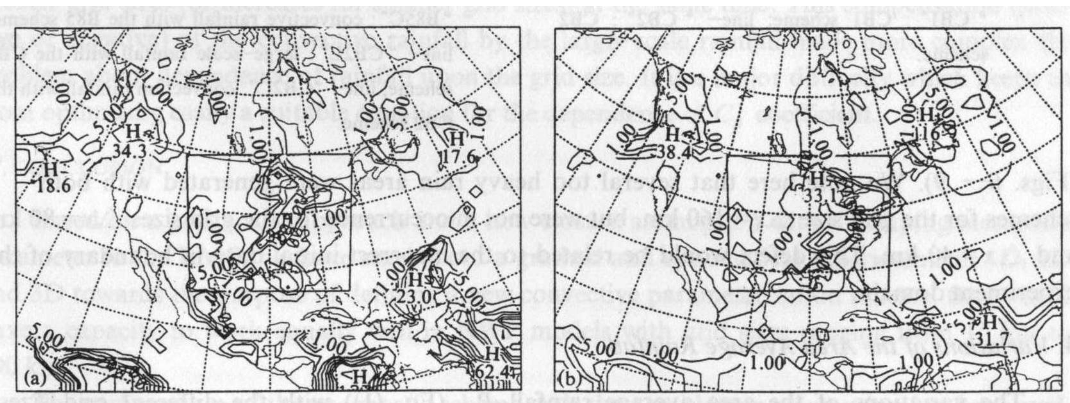

Fig. 8. As in Fig. 7, but for $\triangle x = 80$ km.

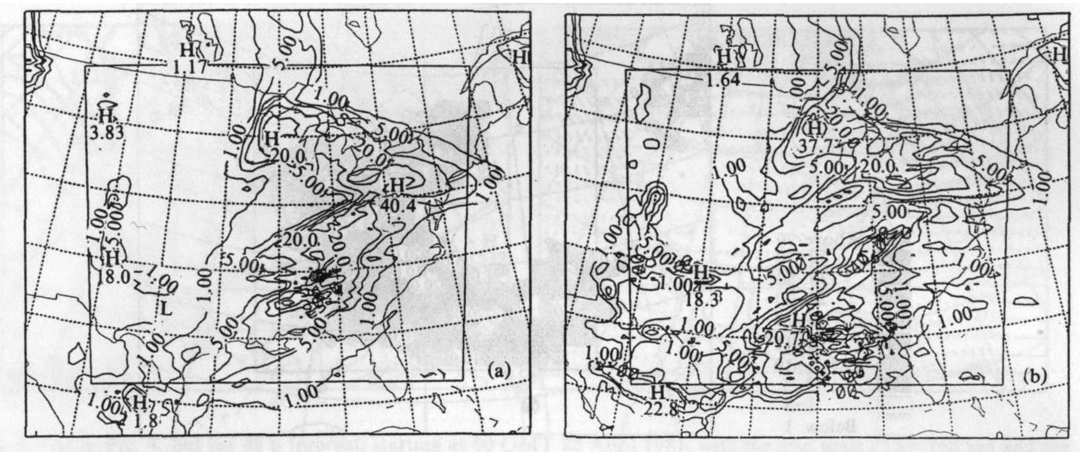

Fig. 9. As in Fig. 7, but for $\triangle x = 40$ km.

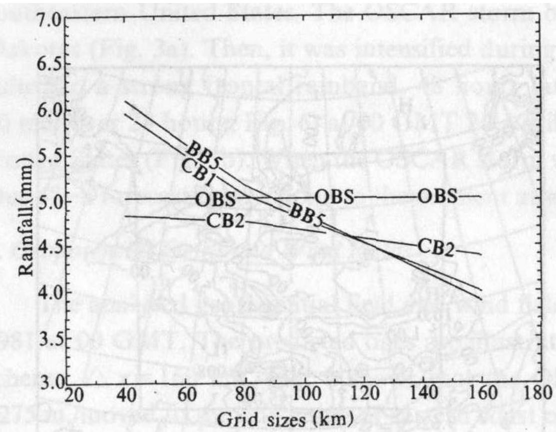

Fig. 10. Variations of the area average 24–h rainfall over the controlling domain with the different grid scales: $\triangle x = 160$ km, $\triangle x = 80$ km, and $\triangle x = 40$ km. Line– " B85" is for the B85 scheme; line– " OBS" : observation; line– " CB1" : CB1 scheme; line– " CB2" : CB2 scheme.

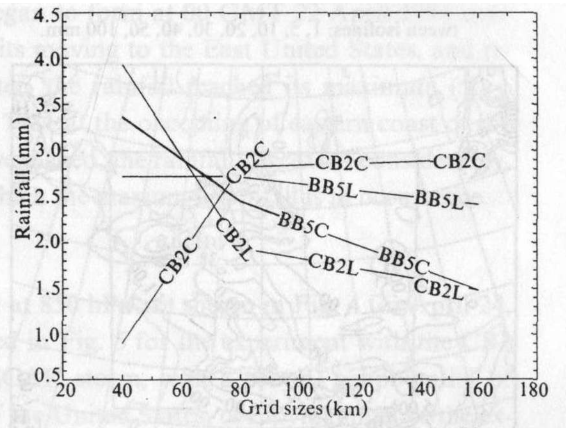

Fig. 11. Variations of the area average 24–h large–scale and convective scale rainfall over the controlling domain with the different grid scales: $\triangle x = 160$ km, $\triangle x = 80$ km, and $\triangle x = 40$ km. Line– "B85L" is for the large–scale rainfall with the B85 scheme; line– "B85C": convective rainfall with the B85 scheme; line– "CB2L": large–scale rainfall with the CB2 scheme; line– "CB2C": convection rainfall with the CB2 scheme.

(Figs. 6— 9). We note here that several too heavy rain areas were generated with both schemes for the grid size $\triangle x = 160$ km, but were not in occurrence for the grid sizes $\triangle x = 80$ km and $\triangle x = 40$ km. This defect would be related to the incorrect initial data in boundary of the experiment domain.

4. *Variations of the Area Average Rainfall*

The variations of the area average rainfall $\overline{R}_p$ (Eq. (1)) with the different grid sizes,

$\triangle x = 160$ km, 80 km and 40 km, were illustrated in Fig. 10, of which numerical values are listed in Table 2. Generally, when the grid sizes decrease, the predicted rainfall increases (Fig. 10). Some limited improvements dealing with the dependence problem of rainfall upon grid sizes could even be done by the CB1 scheme. For this case, the optimum choices of the grid size and the convective parameterization scheme are $\triangle x = 80$ km and the prognostic CB1 scheme (Table 2). But, the CB2 scheme did give a better solution concerning the dependence problem under study (Fig. 10). Indeed, the ratio of the area average rainfall $\overline{R}_p$ between grid sizes $\triangle x = 40$ km and $\triangle x = 160$ km is about 156.6% for the B85 scheme; 149.1% for the CB1 scheme, and 110.3% for the CB2 scheme (Table 2). In other words, when the grid sizes decrease from $\triangle x = 160$ km to $\triangle x = 40$ km, the rainfall increases by 56.6% for the B85 scheme, only 10.3% for the CB2 scheme.

Table 2. Area Average 24–h Rainfall over the Controlling Domain (Observations and Predictions) with Different Grid Scales and Different Convective Parameterization Schemes

Schemes	160 km	40 km	40 km	r_p *
B85	3.89	5.16	6.09	1.566
CB1	3.99	5.05	5.95	1.491
CB2	4.38	4.76	4.83	1.103
observation	—	5.02	—	1.000

* $r_p = \overline{R}_p$ ($\triangle x = 40$ km) / $\overline{R}_p$ ($\triangle x = 160$ km).

5. *Variations of the Large–Scale and Convective Scale Rainfall*

Moreover, it is interesting to separately examine the contributions of the large–scale and convective scale rainfalls, which are illustrated in Fig. 11, to the dependence of total rainfall upon grid sizes. Fig. 11 shows that with the B85 scheme, the large–scale rainfall changes a little with grid sizes, but the convective rainfall is more sensitive to grid sizes. As a consequence, the total rainfall depends upon grid sizes according to the contribution of the convective rainfall. For the case of the CB2 scheme, it is no such apparent. We found that the CB2 scheme can increase much the convective rainfall for greater grid sizes (or decrease for smaller grid sizes) with regard to those obtained by the B85 scheme. However, the large–scale rainfall decreases for greater grid sizes (or increases for smaller grid sizes) at the same time. This compensation (positive or negative) of the convective rainfall by the large–scale rainfall made more complex the problem about dependence of rainfall upon the grid size. It is a major difficulty which keeps us from optimizing easily a suitable equation for the dependence of C_β coefficient.

IV. CONCLUSION

Based on a prognostic approach and a new closure assumption with a damping mesoscale parameter in the RMC, we have carried out a gradual and systematical experiments in 1D, 2D and 3D towards the purpose of defining a new convective parameterization scheme, that would have a capacity to work equally well in NWP models with grid sizes ranging from 10 km to 100 km.

The performance of the prognostic scheme with the new closure assumption has been evaluated by the predictions with the data of the experiment OSCAR. The geopotential field, wind field and rainband associated have been reasonably simulated. Usually, when the grid sizes of the host model decrease, the area average rainfall increases: 56.6% of increasing for the B85 scheme and 10.3% only for the CB2 scheme. It is well obvious for the improvement on this problem by the prognostic scheme with the new closure assumption. That is probably due to the capacity of the latter to induce more mesoscale circulations for greater grid sizes and to reduce (or damp) more large–scale ones for smaller grid sizes. In fact, the vertical integration of Eqs. (2) and (19) (see Chen and Bougeault, 1993) results in

$$\int_{P_b}^{P_t} \frac{\partial \bar{q}}{\partial t} \cdot \frac{dp}{g} = \int_{P_b}^{P_t} K \cdot (q_c - \bar{q}) \cdot \frac{dp}{g} \tag{4}$$

for the B85 scheme and

$$\int_{P_b}^{P_t} \frac{\partial \bar{q}}{\partial t} \cdot \frac{dp}{g} = \int_{P_b}^{P_t} K \cdot (q_c - \bar{q}) \cdot \frac{dp}{g} + \triangle F_q + A_h$$

$$-(C_\beta - 1) \cdot A_v + \frac{\partial \alpha^*}{\partial t} \cdot \int_{P_b}^{P_t} \frac{(h_c - \bar{h})}{L} \cdot \frac{dp}{g} \tag{5}$$

for the prognostic scheme with the new closure assumption, where A_h, A_v and $\triangle F_q$ denote the vertical integrals of the horizontal, vertical advections, and the vertical diffusion flux of moisture. The environmental moistening can be only due to the detrained cloud humidity in the B85 scheme (Eq. (4)). It is also the case with the other Kuo–type schemes (Kuo, 1965; 1974; Anthes, 1977; Geleyn, 1985). On the contrary, in the CB2 scheme, the environmental moistening can be dut to not only the detrained cloud humidity, but also the humidity storage within the clouds, the moisture of the vertical diffusion flux and the horizontal advection. However, The contribution of the term of vertical advection depends upon the C_β coefficient. For smaller grid sizes, the hydrostatic approximation made in most mesoscale models will induce too larger–scale circulation in presence of strong convection, and taking a coefficient smaller than 1 (for example, $\triangle x < 80$ km, $C_\beta < 1$ in our case) might be one way to damp these spurious circulations.

Finally, we would like to indicate that our new prognostic scheme was investigated only in one real situation. It is necessary to examinate it with several different situations for giving a better conclusion.

The authors would like to express their appreciation to R. Rosset and D. Ramond, for their help finding a financial solution to continue this research. We also thank M. Imbard for preparing the initial data input files, Y. H. Kuo and S. Low–Nam for providing the OSCAR rainfall analysis, and J. F. Geleyn for suggesting discussions.

REFERENCES

Anthes, R. A. (1977), A cumulus parameterization scheme utilizing a one–dimensional cloud model, *Mon. Wea. Rev.*, **105**: 270—286.

Bougeault, P. (1985), A simple parameterization of the large–scale effects of cumulus convection, *Mon. Wea. Rev.*, **113**: 2108—2121.

Brière, S. (1982), Nonlinear normal mode initialization of a limited area, *Mon. Wea. Rev.*, **110**: 1116—1186.

Chen Dehui (1989), Adaptation d'un schèma pronostique de parametrisation de la convection à un modèle de prévision numérique à maille variable, *Thèse de Doctorat*, Université Blaise Pascal, 105—117, available from CNRM, 31057 Toulouse, France.

Chen Dehui (1991), Test d'un nouveau schèma de convection pronostique adaptable à un modèle à maille variable.

Note de Travail de la METEO–FRANCE, No. 2, available from CNRM, 31057 Toulouse, France.

Chen Dehui and Bougeault, P. (1993), A simple prognostic closure assumption to deep convective parameterization: I, *Acta Meteor. Sinica*, **7**: 1—18.

Davies, H. C. (1976), A lateral boundary formulation for multi–level prediction models, *Quart. J. Roy. Meteor. Soc.*, **102**: 405—418.

Degardin, P. and Imbard, M. (1987), Evaluation d'une simulation du modèle PERIDOT sur the USA, *Note de Travail de l'EERM N°* 192, 160 pp.

Geleyn, J. F. (1985), On a simple, parameter–free partition between moistening and precipitations in the Kuo scheme, *Mon. Wea. Rev.*, **113**: 405—407.

Geleyn, J. F. (1986), Use of a modified Richardson number for parameterizing the effect of shallow convection *Technical Document*, WMO / TD–No. 114 (Tokyo, 4—8 August 1986).

Geleyn, J. F. et al. (1988), The evolution of numerical weather prediction and atmospheric modelling at the French weather service, *J. Theor. and Appl. Mecha.*, Special Issue, Supplement No. 2, **7**: 87—110.

Imbard, M. et al. (1987), The PERIDOT fine–mesh numerical weather prediction system: description, evaluation and experiments, *J. Meteor. Soc. Japan*, Special NWP Symposium Volume, 455—165.

Krishnamurti, T. N., Low–Nam, S. and Pasch, R. (1983), Cumulus parameterization and rainfall rates II, *Mon. Wea. Rev.*, **111**: 861—828.

Kuo, H. L. (1965), On formation and intensification of tropical cyclones through latent heat release by cumulus convection, *J. Atmos. Sci.*, **22**: 40—63.

Kuo, H. L. (1974), Further studies of the parameterization of the influence of cumulus convection on large–scale flow, *J. Atmos. Sci.*, **31**: 1232—1240.

Kuo, Y. H., Skumanich, M., Haagenson, Ph. L. and Chang, J. S. (1985), The accuracy of trajectory models as showed by the observation system simulation experiments, *Mon. Wea. Rev.*, **113**: 1852—1867.

Louis, J. –F. (1979), A parametric model of vertical eddy fluxes in the atmosphere, *Bound. Layar Meteor.*, **17**: 187—202.